Available online at www.sciencedirect.com
SCIENCE DIRECT®
PERGAMON
Polyhedron 22 (2003) 1191–1198
POLYHEDRON
www.elsevier.com/locate/poly

Structural characterization of a new manganese(III)–salen complex [H_2salen = *N*,*N*′-bis(salicylidene)ethane-1,2-diamine] and study of its electron transfer kinetics with hydroquinone and catechol

Anangamohan Panja [a], Nizamuddin Shaikh [a], Mahammad Ali [b], Pavel Vojtíšek [c], Pradyot Banerjee [a,*]

[a] *Department of Inorganic Chemistry, Indian Association for the Cultivation of Science, Kolkata 700032, India*
[b] *Department of Chemistry, Jadavpur University, Kolkata 700032, India*
[c] *Department of Inorganic Chemistry, Universita Karlova, Albertov 2030, 12840 Prague 2, Czech Republic*

Received 1 May 2002; accepted 10 January 2003

Abstract

The octahedral manganese(III) complex, [Mn(salen)Cl(H_2O)]·H_2O (H_2salen = *N*,*N*′-bis(salicylidene)ethane-1,2-diamine), has been synthesized and structurally characterized by single-crystal X-ray diffraction study. The X-ray structural analysis shows that the metal center is six-coordinate with distorted octahedral geometry. In this compound, the Mn–Cl and Mn–OH_2 bond lengths are 2.621(6) and 2.333(2) Å, respectively, slightly longer than the usual values. The kinetics of electron transfer reaction of the complex with catechol and hydroquinone has been followed spectrophotometrically over the pH range 5.75–8.15 at 30 °C. The nature of the kinetic trace is indicative of a biphasic reaction with each reductant. Detailed analysis of kinetic data supports the formation of a relatively stable intermediate complex between manganese(III) and the dihydroxybenzenes (H_2A) at the initial stage. The decay of the intermediate is the bimolecular electron transfer process involving another molecule of reductants leading to the manganese(II) complex and benzoquinones. Mn^{III}(salen)(H_2O)(OH) generated in situ from the aquation and proton equilibrium of the parent complex has been assigned to be the reactive species during the formation of the intermediate. The corresponding species for the redox step is Mn^{III}(L)(H_2O)(HA), sufficient experimental evidence for which has been gathered from pH-rate profiles.

Keywords: Mn^{III}–Schiff base complex; Crystal structures; Redox activity; Hydroquinone; Catechol

1. Introduction

The Schiff base complexes of manganese(III) are considered to be the simplest models for the reactivity of OEC active site of manganese catalases. Three main structural types for the Schiff base ligand *N*,*N*′-bis(salicylidene)ethane-1,2-diamine (H_2salen) have been reported [1]: (i) mononuclear M(salen)X, where X = halide; (ii) binuclear $[M(salen)]_2$; and (iii) bridged binuclear $[M(salen)O]_2$.

The manganese(III)–salen complex reported by Boucher [2] in powder form shows a magnetic moment value of 4.84 BM (in solid), little below the theoretical spin-only magnetic moment of d^4 high-spin systems. However, no prominent band in the 900–700 cm^{-1} region of IR spectrum was located, and this was attributed to the absence of Mn–O–Mn bridge of the dimer. The Mn^{III}–salen complex reported by Ashmawy et al. [3] was considered to have a dimeric structure. In the absence of a single-crystal X-ray structure, the authors have established it from IR data and antiferromagnetic interactions in the solid state. Supporting evidence has been put forward from fast-atom bombardment mass spectroscopy. On the other hand, conductivity measurements at 295 K lends support for the existence of an equilibrium between monomeric and dimeric formulations as given by

$$2[Mn(salen)(H_2O)]ClO_4 \rightleftharpoons [Mn(salen)(H_2O)]_2(ClO_4)_2 \quad (1)$$

* Corresponding author. Fax: +91-33-2473-2805.
E-mail address: icpb@mahendra.iacs.res.in (P. Banerjee).

0277-5387/03/$ - see front matter
doi:10.1016/S0277-5387(03)00068-8

In the following year, Pecoraro and Butler [4] reported a mononuclear species, [Mn(salen)Cl]CH_3CN, which displays a square-pyramidal geometry similar to that of [Fe^{III}(salen)Cl] [5].

In the attempts [3,6–8] of finding artificial catalysis for the decomposition of water, investigation on the new complexes of manganese(III) with salen [9] and its derivatives [10] is a continuing process. We present here the crystallographic characterization of a new mononuclear manganese(III)–salen complex in a nearly octahedral environment prepared in aqueous methanolic medium. The electron transfer reactivity of this manganese(III) complex with catechol and hydroquinone has also been studied over the pH range 5.75–8.15. Although dihydroxybenzene is not involved in PS II, the intervention of the oxidized (semiquinone) form of this structural element in PS I is reported [11]. The precise mechanism of the reactions is thereby worth pursuing.

2. Experimental

2.1. Materials

Ethylenediamine, salicylaldehyde, hydroquinone, and catechol were of analytical reagent grade (Aldrich) and used without further purification. All other chemicals, e.g. manganous acetate tetrahydrate, manganous chloride, acetonitrile, methanol, sodium hydroxide, and perchloric acid were of reagent grade. Ionic strength and pH were adjusted by $NaClO_4$ (Fluka AR) and NaH_2PO_4 (Fluka AR), respectively. Both were recrystallized before use. Stock solutions were prepared with doubly distilled water.

2.2. Synthesis of the complex

The *trans*-[Mn(salen)Cl(H_2O)]·H_2O complex was prepared through a two-step process, the first step of which involves the preparation of [Mn^{III}(salen)OAc]·H_2O following the standard literature procedure [12]. In the second step, the [Mn^{III}(salen)OAc]·H_2O (0.8 g, 2 mmol) dissolved in methanol (20 cm^3) was mixed well with a solution of $MnCl_2·4H_2O$ (0.4 g, 2 mmol) in water (15 cm^3) which caused an immediate color change from greenish brown to brownish black. The resulting mixture was kept at room temperature for several days. During this period, a dark brownish black microcrystalline compound separated out, which was collected by vacuum filtration and washed with distilled water, followed by diethyl ether to remove excess water. Yield: 0.67 g (85%) (Found: C, 49.2; H, 4.6; N, 7.2. Calc. for $C_{16}H_{18}N_2O_4ClMn$: C, 48.91; H, 4.58; N, 7.13%). FTIR (KBr, cm^{-1}): $\nu_{C=N}$ 1598, ν_{C-O} 1286, ν_{OH} 3404–3448. UV–Vis spectrum (H_2O): λ_{max} (nm) (ε_{max}, mol^{-1} dm^3 cm^{-1}): 213 (sh), 234 (37,600), 279 (17,100), 300 (sh), 386 (sh). μ_{eff} 4.94 BM.

2.3. Physical measurements

Microanalysis (CHN) was performed by a Perkin–Elmer 240C elemental analyzer. pH measurements were made with a Systronics digital pH meter (model 335, India). Magnetic susceptibility measurement was carried out on a PAR 155 vibrating sample magnetometer, and the EPR spectra were obtained on a Varian model 109 E-line X-band spectrometer equipped with a low-temperature quartz Dewar for measurements at 77 K. IR spectra were obtained on a Nicolet, MAGNA-IR 750 spectrometer with samples prepared as KBr pellets. Conductivity measurements were made with Systronics (India) direct reading conductivity meter (model 304). Cyclic voltammetry was performed at a planar EG&G PARC G0229 glassy carbon millielectrode using an EG&G PARC electrochemical analysis system (model 250/5/0) in acetonitrile under dry nitrogen atmosphere in conventional three-electrode configurations with a scan rate of 0.05 V s^{-1}.

Spectral and kinetic measurements were performed in a UV–Vis Spectrophotometer (UV-2100, Shimadzu, Japan). The reactions were initiated by injecting a constant proportion of the complex into the solution containing the substrate, buffer, and $NaClO_4$ (for maintaining ionic strength at 0.2 mol dm^{-3}) according to the conditions required. Dilute solutions of NaOH and $HClO_4$ were used to adjust the pH to a desired value. Although the measured pH is defined by the activity of the hydrogen ion, the concentration of hydrogen ion in terms of $-\log[H^+]$ for each solution was obtained by calibrating the pH-electrode with analytically prepared solutions to the desired ionic strength. The reactions were studied under pseudo-first-order conditions at 400 nm taking the complex as a minor component. The corresponding rate constants were evaluated by means of suitable nonlinear acquisition analysis system with data taken for at least three half-lives of the reactions.

2.4. Crystal structure determination and structural refinement of *trans*-[Mn(salen)Cl(H_2O)]·H_2O

Single crystals of *trans*-[Mn(salen)Cl(H_2O)]·H_2O were obtained by recrystallization of the complex from methanol–water mixture. Data were collected by ω-scan method in the 2θ range 3.2°–27.5° on an Enraf-Nonious CAD4 diffractometer with graphite-monochromated Mo Kα radiation ($\lambda = 0.71070$ Å) at 293 K. Information concerning crystallographic data collection and refinement of the structure is compiled in Table 1. Unit-cell parameters and orientation matrix were determined by a least-squares fit. Intensity data were

Table 1
Data collection and structure refinement of *trans*-[Mn(salen)Cl(H_2O)]·H_2O

Empirical formula	$C_{16}H_{18}N_2O_4ClMn$
Formula weight	392.71
Crystal system	monoclinic
Space group	$P2_1/n$
Unit cell dimensions	
a (Å)	6.6470(2)
b (Å)	7.3330(2)
c (Å)	33.8260(10)
β (°)	95.1650(17)
V (Å^3)	1642.07(8)
Z	4
μ(Mo Kα) (mm^{-1})	0.990
T (K)	293
Total data	6921
Unique data, R_{int}	3320(0.023)
Data [$I > 2\sigma(I)$]	3080
R [$I > 2\sigma(I)$]	0.0332
wR [$I > 2\sigma(I)$]	0.0811

corrected for Lorentz polarization but not for absorption. All calculations for structure solution and refinement were done by standard procedures (SHELXS-97 [13] and SHELXL-97 [14]). All non-hydrogen atoms were refined anisotropically by full-matrix least-squares techniques on F^2. All the hydrogen atoms were located in Fourier difference maps and refined isotropically. The final crystal structure was drawn using ORTEP program [15].

3. Results and discussion

3.1. Description of the structure of [Mn(salen)Cl(H_2O)]·H_2O

An ORTEP view of the complex with atom numbering scheme is shown in Fig. 1 and the important bond distances and angles are summarized in Table 2. In this monomeric complex, the manganese atom displays a slightly distorted octahedral coordination in which manganese(III) ion is being displaced from the O(1), N(1), N(2), O(2) planes by 0.066 Å. The nearly planar tetradentate salen ligand is tightly bound to manganese(III) ion via N_{imine} and O_{phenol} atoms (Mn–N_{imine} bond lengths of 1.985(17) and 1.982(17) Å, and the Mn–O_{phenol} bond lengths of 1.864(14) and 1.901(15) Å). The distortion of the coordination octahedron is due to the slight difference (0.037 Å) between the Mn–O(1) and Mn–O(2) bond lengths as well as between O(1)–Mn–N(1) and O(2)–Mn–N(2) bond angles (0.72°). Slight deviation of N(2)–Mn–N(1) axis from orthogonality (82.45(7)°) to equatorial plane is also noteworthy. However, the N–Mn–N and O–Mn–N bond angles are typical of metal complexes with salen as a ligand.

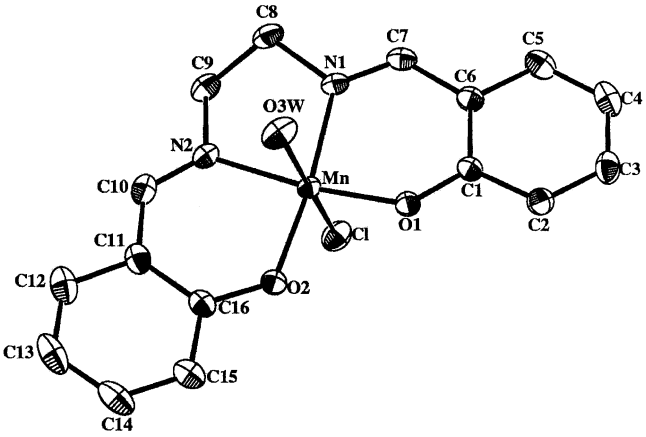

Fig. 1. Molecular structure of the complex *trans*-[Mn(salen)Cl(H_2O)]·H_2O showing the atom labeling scheme. Hydrogen atoms and solvent water molecule have been omitted for clarity.

The Mn^{III}–Cl bond length in square-pyramidal [Mn^{III}(salen)Cl] [4] is 2.461 Å with manganese(III) ion being displaced by 0.19 Å above the equatorial plane, whereas in this octahedral complex the Mn^{III}–Cl and Mn–OH_2 bond lengths are 2.621(6) and 2.333(17) Å, respectively, which are little longer than usual values [10] probably due to the hydrogen bonds (Fig. 2). The coordinated Cl ion takes part in two H bonds with

Table 2
Selected bond distances (Å) and bond angles (°) for complex *trans*-[Mn(salen)Cl(H_2O)]·H_2O

Bond distances	
Mn–Cl	2.6209(6)
Mn–O(1)	1.8641(14)
Mn–O(2)	1.9010(15)
Mn–O(3W)	2.3329(17)
Mn–N(1)	1.9846(17)
Mn–N(2)	1.9818(17)
Bond angles	
Cl–Mn–O(1)	94.71(5)
Cl–Mn–O(2)	95.50(5)
Cl–Mn–O(3W)	174.08(5)
Cl–Mn–N(1)	87.44(5)
Cl–Mn–N(2)	89.60(5)
O(1)–Mn–O(2)	93.73(6)
O(1)–Mn–O(3W)	88.96(7)
O(1)–Mn–N(1)	91.42(7)
O(1)–Mn–N(2)	172.35(6)
O(2)–Mn–O(3W)	88.89(7)
O(2)–Mn–N(1)	173.83(7)
O(2)–Mn–N(2)	92.14(7)
O(3W)–Mn–N(1)	87.82(7)
O(3W)–Mn–N(2)	86.26(6)
N(1)–Mn–N(2)	82.44(7)
Bond distances	
O(3W)···O(4W)	2.808(3)
O(3W)···Cl	3.261(17)
O(4W)···O(2)	2.936(3)
O(4W)···Cl	3.251(2)

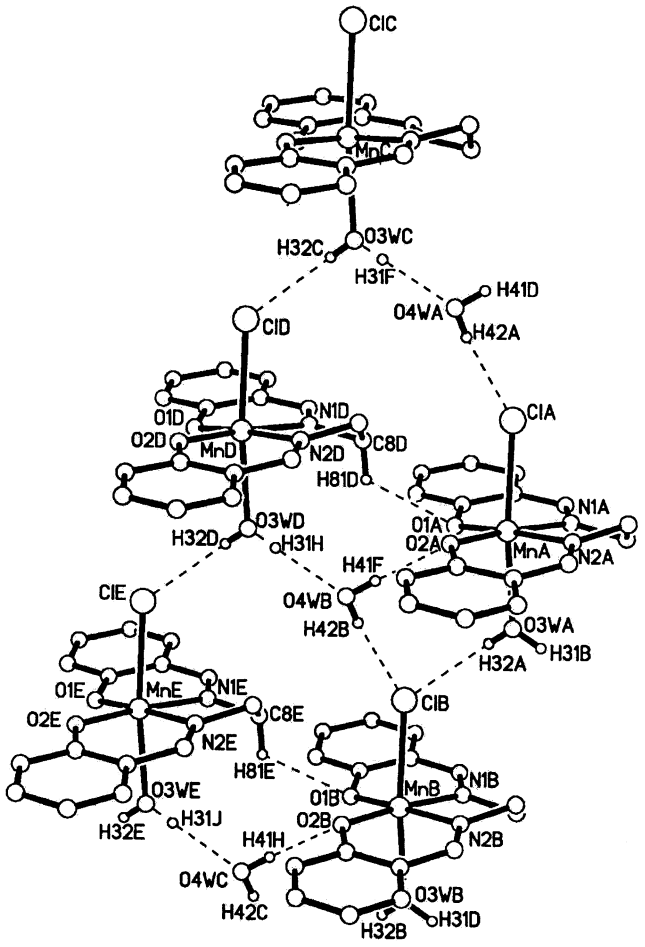

Fig. 2. Molecular packing diagram showing intermolecular hydrogen bonding in $[Mn(salen)Cl(H_2O)]\cdot H_2O$.

O3W and O4W (O3W···Cl: 3.261 Å and O4W···Cl: 3.251 Å) from the next unit-cell. On the side of Mn–salen plane, the Mn–OH_2 bond is affected by two hydrogen bonds (O3W···O4W: 2.808 Å). The elongation from 2.461 to 2.621 Å definitely points to a very weak bonding of Mn^{III}–Cl in the octahedral environment, and supports the observation that when dissolved in water (or in polar solvent such as CH_3CN), the dissociation of chloride occurs instantaneously producing a 1:1 electrolyte (molar conductance, 110 Ω^{-1} cm^2 mol^{-1}) presumably due to the formation of $[Mn(salen)(H_2O)_2]^+$ complex. The packing diagram reveals a three-dimensional framework due to four intermolecular hydrogen bonds involving [Mn(salen)Cl(H_2O)] molecules. Non-coordinated water molecules also participate in this framework. The ligands (salen) are nearly planar, parallel, and form endless "piles" parallel with the *b*-axis. The distances between them are about 6.76 Å with the Mn–Mn distances of 7.333(2) Å. Thus, no appreciable magnetic interaction is expected in the solid state and the observed magnetic data (4.94 BM) is consistent with the purely monomeric structure of the complex.

3.2. Cyclic voltammetric studies

The cyclic voltammetric study on $[Mn^{III}$(salen)Cl(H_2O)] was carried out in acetonitrile medium using a three-electrode assembly consisting of a glassy carbon working electrode, a platinum counterelectrode, and a saturated calomel as reference electrode. The cyclic voltammogram is depicted in Fig. 3. In this case, the metal center reduction takes place quasi-reversibly as evidenced from the fact that the peak-to-peak separation, ΔE_p, is 75 ± 5 mV. $E_{1/2}$ of the complex was determined to be -0.237 V vs. SCE, which is higher than that observed in the complex $[Mn^{III}$(salen)Cl] ($E_{1/2} = -0.264$ V at a scan rate of 50 mV s^{-1}).

3.3. Spectrophotometric determination of pK of $[Mn^{III}(salen)(H_2O)_2]^+$

Spectral change observed during the reaction of the Mn^{III} complex with H_2A (where H_2A represents the generalized form of both hydroquinone (H_2Q) and catechol (H_2cat)) at pH 7.00 showed an initial increase in absorbance followed by a decay (Fig. 4). The initial increase in absorbance may be due to the formation of an intermediate, which then undergoes redox transformation. This observation prompted us to determine spectrophotometrically the pK_m of the complex $[Mn^{III}(salen)(H_2O)_2]^+$ which is actually generated in situ from $[Mn^{III}(salen)(Cl)(H_2O)]$ in aqueous solution. For this purpose, a fixed concentration of the complex (5.0×10^{-5} mol dm^{-3}) was allowed to react with 0.003 mol dm^{-3} of H_2Q over a wide pH range 5.0–8.15. The maximum absorbance at 400 nm was noted and plotted against $[H^+]$ (Fig. 5). It is apparent that the concentration of the intermediate complex decreases with the increase in pH until it reaches ~ 6.00, below which no detectable amount of the intermediate is formed. It also appears that $[Mn^{III}(salen)(H_2O)_2]^+$ does not form any intermediate, and $[Mn^{III}(salen)(H_2O)(OH)]$, owing to the enhanced lability of the aqua group having a OH^-

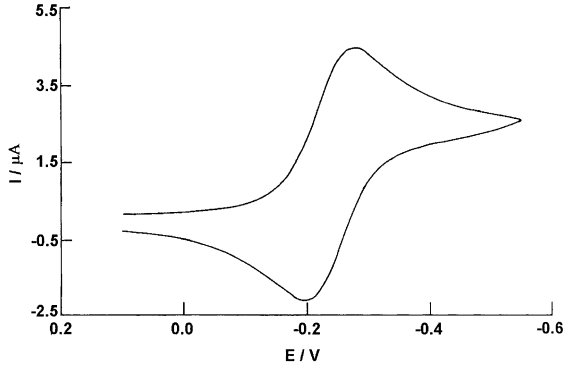

Fig. 3. Cyclic voltammogram of *trans*-$[Mn(salen)Cl(H_2O)]\cdot H_2O$, 1.0×10^{-3} mol dm^{-3}, in acetonitrile with 0.1 mol dm^{-3} TEAP, and scan rate of 50 mV s^{-1} measured at a glassy carbon electrode.

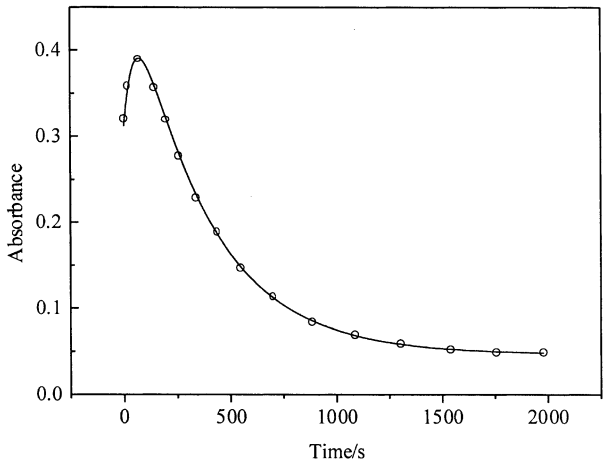

Fig. 4. Absorbance vs. time graph (400 nm) for the reduction of $[Mn^{III}(salen)(H_2O)_2]^+$ (5.0×10^{-5} mol dm^{-3}) with H_2Q (4×10^{-3} mol dm^{-3}) at 30 °C, pH 7.00, $I = 0.2$ mol dm^{-3} ($NaClO_4$), and 0.05 mol dm^{-3} phosphate buffer. (—) Best fit curve and (○) experimental points.

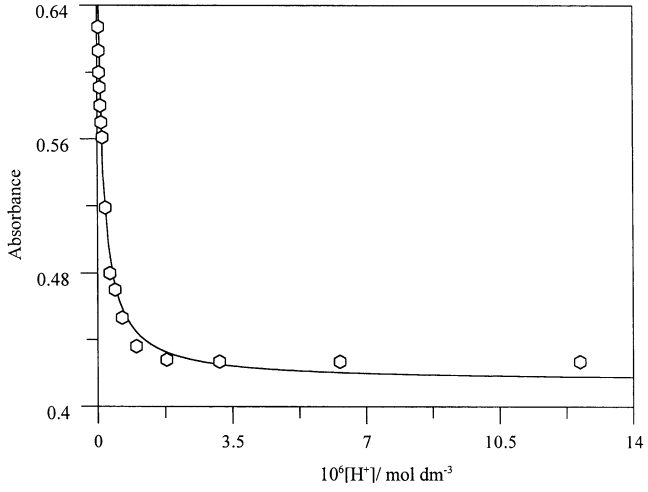

Fig. 5. Plot of absorbance vs. $[H^+]$ for the spectrophotometric determination of pK_m of $[Mn^{III}(salen)(H_2O)_2]^+$ (5.0×10^{-5} mol dm^{-3}) at 30 °C, $[H_2Q] = 3 \times 10^{-3}$ mol dm^{-3}, $I = 0.2$ mol dm^{-3} ($NaClO_4$), and 0.05 mol dm^{-3} phosphate buffer.

in the *trans*-position, forms the intermediates with H_2A. This can be expressed as

$$[Mn^{III}(L)(H_2O)_2]^+ \overset{K_m}{\rightleftharpoons} [Mn^{III}(L)(H_2O)(OH)] + H^+ \quad (2)$$

$$[Mn^{III}(L)(H_2O)(OH)] \overset{HA^-}{\rightleftharpoons} [Mn^{III}(L)(HA)(OH)]^- + H_2O \quad (3)$$

$$[Mn^{III}(L)(H_2O)(OH)] \overset{H_2A}{\rightleftharpoons} [Mn^{III}(L)(H_2A)(OH)]^- + H_2O \quad (4)$$

where L denotes salen. This change in absorbance with pH allows to determine the pK_m of the complex $[Mn^{III}(L)(H_2O)_2{}^+]$ by using the equation

$$A = \frac{A_{H_2O}[H^+] + K_m A_{OH^-}}{K_m + [H^+]} \quad (5)$$

where A_{H_2O} is the absorbance of the complex when it is in 100% aqua form. A_{OH^-} is the absorbance of the complex when it is in 100% hydroxo form that leads to the formation of the intermediate in 100% yield. A is the absorbance of the complex in between the two extreme conditions where both A_{H_2O} and A_{OH^-} exist. A non-linear fit of the experimental data to Eq. (5) by means of a computer-fit program gives the value of $K_m = (1.23 \pm 0.16) \times 10^{-7}$ (p$K_m = 6.91$). The same results could be extracted from reactions involving manganese(III) complex and H_2cat.

3.4. Stoichiometry and reaction products

The stoichiometry of the reaction was determined by reacting fixed and excess concentration of complex, varying the concentration of the H_2A and then estimating the unreacted concentration of the complex spectrophotometrically at 400 nm and pH 7.00. These measurements confirm the following stoichiometric reactions:

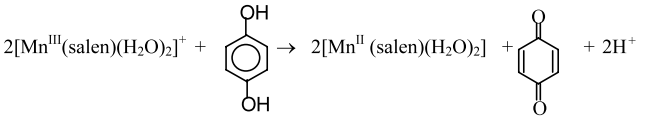

(6)

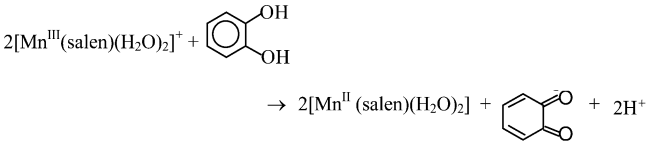

(7)

The formation of *ortho*- and *para*-benzoquinones was confirmed by IR and ^{1}H NMR spectroscopy of the isolated products. The reduction product of the complex is the corresponding Mn^{II} species and was confirmed by EPR measurement showing 6-line EPR signals.

3.5. Description of the reactivity of the system

Under the pseudo-first-order reaction condition, the absorbance (A_t) vs. t curve shows an exponential increase followed by an exponential decay. These observations indicate that the oxidation of H_2A occurs through the formation of a relatively stable intermediate followed by its redox decomposition and can be represented by the following sequence of reactions:

$$A \underset{k_0(-1)}{\overset{k_0(1)}{\rightleftharpoons}} B \overset{k_0(2)}{\rightarrow} C \quad (8)$$

$k_0(1)$, $k_0(-1)$, and $k_0(2)$ were evaluated by fitting the

Table 3
Pseudo-first-order rate constants $k_0(1)$ [a] for the formation of intermediate complexes and $k_0(2)$ [a] for the redox decomposition of intermediate complexes by dihydroxybenzenes at 30 °C, pH 7.00, $I = 0.2$ mol dm^{-3} ($NaClO_4$), and 0.05 mol dm^{-3} phosphate buffer [a]

$[H_2A]_T$ ($\times 10^3$ mol dm^{-3})	$k_0(1)$ ($\times 10^3$ s^{-1})		$k_0(2)$ ($\times 10^3$ s^{-1})	
	H_2Q	H_2cat	H_2Q	H_2cat
0.70	5.21 ± 0.02	–	6.20 ± 0.08	–
1.0	7.23 ± 0.03	1.28 ± 0.06	9.04 ± 0.06	4.83 ± 0.04
2.0	14.5 ± 0.11	–	18.1 ± 0.04	–
3.0	23.5 ± 0.05	2.12 ± 0.03	26.5 ± 0.08	9.62 ± 0.04
4.0	31.6 ± 0.04	3.09 ± 0.02	28.9 ± 0.06	13.7 ± 0.09
5.0	39.8 ± 0.08	–	32.4 ± 0.12	–
6.0	46.2 ± 0.12	3.62 ± 0.05	33.0 ± 0.02	16.3 ± 0.06
7.0	54.2 ± 0.22	–	33.7 ± 0.11	–
8.0	59.3 ± 0.10	4.41 ± 0.08	34.9 ± 0.13	18.1 ± 0.12
10	72.6 ± 0.26	5.95 ± 0.04	35.9 ± 0.09	18.8 ± 0.10
20	–	10.3 ± 0.09	–	23.8 ± 0.04
40	–	18.8 ± 0.12	–	28.7 ± 0.08
60	–	31.3 ± 0.08	–	31.7 ± 0.09

[a] $k_0(-1)$ in each trace as computed from KFSIM40 program is $< 10^{-5}$ s^{-1} and not shown.

experimental trace to the above sequence of reactions using KFSIM40 program [16]. The inputs for the program are the A_t vs. t data along with molar absorption coefficients (ε) for A and B together with that of C, and Fig. 4 demonstrates such a typical fit.

3.6. Kinetics of the formation of intermediate complexes

Dependence of the pseudo-first-order rate constants $k_0(1)$ on $[H_2A]$ was investigated at 30 °C, pH 7.0 (0.05 mol dm^{-3} phosphate buffer), and $I = 0.2$ mol dm^{-3} ($NaClO_4$). Plot of $k_0(1)$ vs. $[H_2A]$ is a straight line (Table 3) with slope (7.39 ± 0.16 dm^3 mol^{-1} s^{-1} for H_2Q and 0.49 ± 0.01 dm^3 mol^{-1} s^{-1} for H_2cat) and a small intercept ($8.78 \pm 8.72 \times 10^{-4}$ s^{-1} for H_2Q and $6.59 \pm 3.39 \times 10^{-4}$ s^{-1} for H_2cat), although not significant or precise, can be attributed to contributions from the reverse reaction and/or self decomposition of the parent complex in the medium. To check the effect of pH on the rate of the reaction, kinetic experiments were conducted in the pH range 5.75–7.60 at $[H_2Q] = 0.003$ mol dm^{-3}, $[H_2cat] = 0.004$ mol dm^{-3}, and other conditions were same. $k_0(1)$ vs. $-\log[H^+]$ plot (Fig. 6) shows that the rate of the formation of the intermediate increases slowly at lower pH region and then rises steeply. The above observation can be explained by Eqs. (10)–(13):

$$H_2A \overset{K_a}{\rightleftharpoons} HA^- + H^+ \quad (9)$$

$$[Mn^{III}(L)(H_2O)_2]^+ \overset{K_m}{\rightleftharpoons} [Mn^{III}(L)(H_2O)(OH)] + H^+ \quad (10)$$

$$[Mn^{III}(L)(H_2O)(OH)] + H_2A \underset{k_{-1}}{\overset{k_1}{\rightleftharpoons}} [Mn^{III}(L)(\underset{\Updownarrow}{OH})(H_2A)] + H_2O \quad (11)$$

$$[Mn^{III}(L)(OH)(HA)]^- + H^+ \overset{K_m}{\rightleftharpoons} [Mn^{III}(L)(H_2O)(HA)] \quad (12)$$

$$[Mn^{III}(L)(H_2O)(OH)] + HA^- \underset{k_{-2}}{\overset{k_2}{\rightleftharpoons}} [Mn^{III}(L)(OH)(HA)]^- + H_2O \quad (13)$$

The corresponding rate law is

$$k_0(1) = \frac{k_1[H^+] + k_2K_a}{K_a + [H^+]} \left\{ \frac{K_m}{K_m + [H^+]} \right\} [H_2A]_T + \frac{k_{-1}[H^+] + K'_m k_{-2}}{K'_m + [H^+]} \quad (14)$$

$[H_2A]_T$ is the total analytical concentration of H_2A.

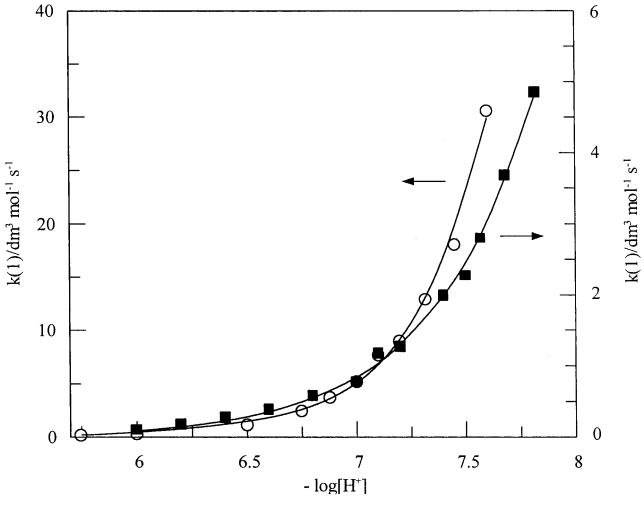

Fig. 6. Plot of second-order rate constants vs. $-\log[H^+]$ for the formation of intermediate complex at 30 °C, $I = 0.02$ mol dm^{-3} ($NaClO_4$), and 0.05 mol dm^{-3} phosphate buffer. (○) For H_2Q (0.003 mol dm^{-3}) and (■) for H_2cat (0.004 mol dm^{-3}); best fit curve is shown by (—).

$k_0(-1)$, the observed rate constant for the backward reaction extracted through KFSIM40 program, is $<10^{-5}$ s^{-1} and almost same in magnitude in each case. This is associated with the second term of the above equation and can be neglected leading to

$$k_0(1) = \frac{k_1[H^+] + k_2K_m}{K_a + [H^+]}\left\{\frac{K_m}{K_m + [H^+]}\right\}[H_2A]_T \quad (15)$$

The above equation was solved by means of a nonlinear least-squares program and the computed parameters for H_2Q are $k_1 = 21.79 \pm 0.49$ dm^3 mol^{-1} s^{-1}, $k_2 = (1.37 \pm 0.21) \times 10^3$ dm^3 mol^{-1} s^{-1}, $K_a = (1.05 \pm 0.17) \times 10^{-9}$, and $K_m = (1.62 \pm 0.29) \times 10^{-8}$. The corresponding values for H_2cat are $k_1 = 1.94 \pm 0.41$ dm^3 mol^{-1} s^{-1}, $k_2 = (2.21 \pm 0.29) \times 10^2$ dm^3 mol^{-1} s^{-1}, $K_a = (3.15 \pm 0.43) \times 10^{-10}$, and $K_m = (4.62 \pm 0.29) \times 10^{-8}$.

3.7. Kinetics of the redox decomposition of the intermediate

An analysis of the kinetic data from the second stage of the reaction demonstrates that the plot of $k_0(2)$ vs. $[H_2A]$ shows a first-order dependence on $[H_2A]$ (Table 3) with no intercept on the rate axis. A rate saturation is, however, noted at higher concentrations of H_2A. The intramolecular electron transfer thereby cannot be a reasonable explanation and the pre-equilibrium formation of a second adduct between the intermediate and the H_2A/HA^- species followed by electron transfer is implicated.

The theoretical rate law is

$$k_0(2) = \frac{2k_2Q[H_2A]_T}{1 + Q[H_2A]_T} \quad (16)$$

where k_2 is the second-order rate constant for the decay step of the reactions and Q the association constant of the second adduct.

The values of k_2 and Q were evaluated by fitting the experimental data to Eq. (16) and the evaluated parameters are $k_2 = (5.00 \pm 0.02) \times 10^{-3}$ dm^3 mol^{-1} s^{-1} and $Q = (2.93 \pm 0.12) \times 10^2$ dm^3 mol^{-1} for H_2Q, and $k_2 = (3.40 \pm 0.07) \times 10^{-3}$ dm^3 mol^{-1} s^{-1} and $Q = (1.42 \pm 0.20) \times 10^2$ dm^3 mol^{-1} for H_2cat at a fixed pH (7.00).

The pH variation study for the electron transfer step shows a bell-shaped curve (Fig. 7) which indicates that $Mn^{III}(L)(H_2O)(HA)$ is the reactive intermediate. Analogous observations were encountered in the oxidation of several inorganic and organic species by $[Mn^{III}(cdta)(H_2O)]^-$, where $[Mn^{III}(cdta)(H_2O)(OH)]^{2-}$, , the hydroxo complex, was found to be redox-inactive [17]. A reasonable reaction scheme thereby can be framed as

$$[Mn^{III}(L)(H_2O)(HA)] \overset{K'_m}{\rightleftharpoons} [Mn^{III}(L)(OH)(HA)]^- + H^+ \quad (17)$$

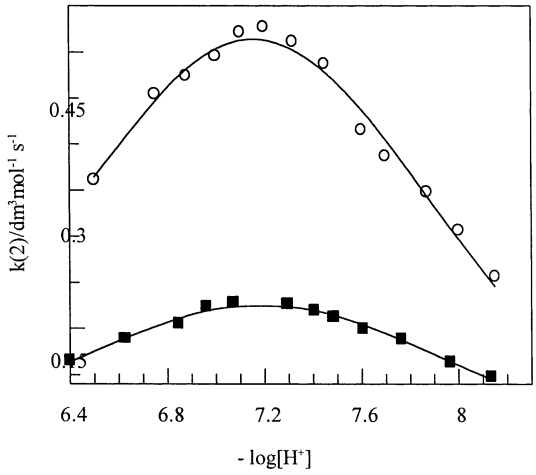

Fig. 7. Plot of second-order rate constants vs. $-\log[H^+]$ for the redox decomposition of intermediate complex by dihydroxybenzenes at 30 °C, $I = 0.02$ mol dm^{-3} ($NaClO_4$), and 0.05 mol dm^{-3} phosphate buffer. (○) For H_2Q (0.003 mol dm^{-3}) and (■) for H_2cat (0.004 mol dm^{-3}); best fit curve is shown by (—).

$$[Mn^{III}(L)(H_2O)(HA)] + H_2A \overset{Q_1}{\rightleftharpoons} IP_1 \overset{k_1}{\rightarrow} Mn^{II} + HA^o + H^+ \quad (18)$$

$$[Mn^{III}(L)(H_2O)(HA)] + HA^- \overset{Q_2}{\rightleftharpoons} IP_2 \overset{k_2}{\rightarrow} Mn^{II} + HA^o \quad (19)$$

The radicals thus generated react in a fast step with another molecule of complex to give the final oxidation products as benzoquinones.

The rate law derived from the above scheme is

$$k(2) = \frac{k_1Q_2[H^+] + k_2Q_2K_a}{K_a + [H^+]}\left\{\frac{H^+}{K'_m + [H^+]}\right\} \quad (20)$$

Here, $k(2) = k_0(2)/2[H_2A]_T$, 2 being the stoichiometric factor of the reactions.

H_2A is always less reactive than its deprotonated form due to the change in the oxidation potential value [18], and its contribution towards the redox step can be assumed to be negligible. It is also evident from the fact that fitting of the experimental data to Eq. (20) gives a negative value for k_1. Thus, Eq. (20) can be reduced to Eq. (21) neglecting the k_1 path as

$$k(2) = \frac{k_2Q_2K_a}{K_a + [H^+]}\left\{\frac{[H^+]}{K'_m + [H^+]}\right\} \quad (21)$$

The evaluated parameters are $k_2Q_2 = 0.77 \pm 0.05$ dm^3 mol^{-1} s^{-1}, $K_a = (2.01 \pm 0.25) \times 10^{-8}$, and $K'_m = (2.39 \pm 0.36) \times 10^{-7}$ for H_2Q; and $k_2Q_2 = 0.38 \pm 0.03$ dm^3 mol^{-1} s^{-1}, $K_a = (1.94 \pm 0.25) \times 10^{-8}$, and $K'_m = (1.28 \pm 0.18) \times 10^{-7}$ for H_2cat.

It is worth noting that the proton dissociation constants (K_a) for H_2A are found to be slightly higher in contrast to the reported value [19] and could be due to the fact that on association the phenolic proton becomes slightly labile. The pK_m value for the complex $[Mn^{III}(L)(H_2O)_2]^+$ obtained by spectrophotometric

method agrees well to the kinetically evaluated value in the formation step.

The interaction of H_2A with the complex $[Mn^{III}(L)(Cl)(H_2O)]$ occurs through the initial formation of relatively stable intermediates which then react with another molecule of H_2A leading to the formation of the final products, manganese(II) and 1,4- or 1,2-benzoquinones. This proposition of the sequence of reactions is supported by the kinetic traces. Similar behavior was also observed in the oxidation of ascorbic acid [20] and sulfur(IV) [21] by the complex $[Mn^{III}(L)(H_2O)_2]^+$. The formation reactions have been shown to be much faster than the decay steps in earlier studies. The reactions reported here are much more complicated, and the formation steps are only about 2–4 times higher than the decay ones.

Several interesting aspects in this study deserve special mention.

1) The complex $[Mn^{III}(salen)(Cl)(H_2O)]$ is octahedral in the solid state as evidenced from its single-crystal X-ray analysis, with the coordinated water molecule being moved far away from the metal center. This is different from the studies reported earlier where it was assumed to have a square-pyramidal structure.
2) The cyclic voltammetric studies showed that the prepared complex has a significantly higher $E_{1/2}$ value compared to the previously reported values on related complexes. This implies that in the later complexes the metal center was coordinatively unsaturated and had natural tendency to dimerise to fulfil the coordination number 6.
3) The oxidation of L-ascorbic acid by $[Mn^{III}(salen)(H_2O)_2]^+$ was found to be inner-sphere in nature leading to the formation of intermediate ascorbate complex which was believed to inhibit the electron transfer act. The observations in the present study are also in the same line but the pH-rate profiles for the redox step clearly point out that it is the protic equilibrium (17) responsible for such observations rendering $[Mn^{III}(L)(OH)(HA)]^-$ to be a silent partner towards redox act.
4) Comparison of reactivity showed that H_2Q is more reactive than H_2cat for both the formation and decay steps which is at par with the earlier findings [22].

4. Supplementary data

Crystallographic data for the structural analysis have been deposited with the Cambridge Crystallographic Data Centre, CCDC No. 168827 for $[Mn^{III}(salen)(Cl)(H_2O)]\cdot H_2O$. Copies of this information may be obtained free of charge from The Director, CCDC, 12 Union Road, Cambridge, CB2 1EZ, UK (fax: +44-1223-336033; e-mail: deposit@ccdc.cam.ac.uk or www: http://www.ccdc.cam.ac.uk).

Acknowledgements

This work has been supported through a research project from the Council of Scientific and Industrial Research, New Delhi, to P.B. and a CSIR–NET fellowship to A.P. We would like to thank Prof. R. Banerjee, Jadavpur University, Kolkata, for some help in operating the KFSIM40 program.

References

[1] M.D. Hobday, T.D. Smith, Coord. Chem. Rev. 9 (1972) 311.
[2] L.J. Boucher, J. Inorg. Nucl. Chem. 36 (1974) 531.
[3] F.M. Ashmawy, C.A. McAuliffe, R.V. Parish, J. Tames, J. Chem. Soc., Dalton Trans. (1985) 1391.
[4] V.L. Pecoraro, W.M. Butler, Acta Crystallogr., Sect. C 42 (1986) 1151.
[5] M. Gerloch, F.E. Mabbs, J. Chem. Soc. A (1967) 1598.
[6] R. Ramraraj, A. Kira, M. Kaneko, Angew. Chem., Int. Ed. Engl. 25 (1986) 825.
[7] J. Limburg, J.S. Vrettos, L.M. Liable-Sands, A.L. Rheingold, R.H. Crabtree, G.W. Brudvig, Science 283 (1999) 1524.
[8] N. Auranzeb, C.E. Helme, C.A. McAuliffe, R.G. Pritchard, M. Watkinson, R. Bermejo, A. Sousa, J. Chem. Soc., Chem. Commun. (1994) 1153.
[9] K. Oyaizu, T. Nakagawa, E. Tsuchida, Inorg. Chim. Acta 305 (2000) 184.
[10] M. Maneiro, M.R. Bermejo, A. Sousa, M. Fondo, A.M. Gonzalez, A. Sousa-Pedrares, C.A. McAuliffe, Polyhedron 19 (2000) 47.
[11] G.W. Brudvig, W.F. Beck, J.C. de Paula, Annu. Rev. Biophys. Chem. 18 (1989) 25.
[12] A. van den Bergen, K.S. Murray, M.J. O'Connor, B.O. West, Aust. J. Chem. 22 (1969) 39.
[13] G.M. Sheldrick, Acta Crystallogr., Sect. A 46 (1990) 467.
[14] G.M. Sheldrick, SHELXL-97, Program for Crystal Structure Refinement, University of Göttingen, 1997.
[15] C.K. Johnson, M.N. Burnett, ORNL-6895, Oak Ridge National Laboratory, Oak Ridge, TN, 2000.
[16] (a) A. Barshop, R.F. Wren, C. Frieden, Anal. Biochem. 130 (1983) 134;
(b) B. Chaudhuri, R. Banerjee, J. Chem. Soc., Dalton Trans. (1998) 3451.
[17] S. Gangopadhyay, M. Ali, P. Banerjee, Coord. Chem. Rev. 135/136 (1994) 399.
[18] S. Bhattacharya, A. Chakravorty, Comments Inorg. Chem. 4 (1985) 1.
[19] B. Saha, A. Dutta, P. Banerjee, Coord. Chem. Rev. 170 (1998) 47.
[20] I.A. Salem, A.H. Gemeay, Transition Met. Chem. 21 (1996) 130.
[21] A.C. Dash, A. Das, Int. J. Chem. Kinet. 31 (1999) 627.
[22] (a) J.C. Brodovitch, A. McAuley, T. Oswald, Inorg. Chem. 21 (1982) 3442;
(b) E. Pelizzetti, E. Mentasi, C. Baiocchi, J. Chem. Soc., Dalton Trans. (1977) 132.